Advanced Powder Technology xxx (xxxx) xxx

Contents lists available at ScienceDirect

Advanced Powder Technology

journal homepage: www.elsevier.com/locate/apt

Original Research Paper

Evaluation and control of the adhesiveness of cohesive calcium carbonate particles at high temperatures

Genki Horiguchi [a], Hidehiro Kamiya [a,*], Pablo García-Triñanes [b]

[a] Department of Chemical Engineering, Tokyo University of Agriculture and Technology, 2-24-16 Naka-cho, Koganei, Tokyo 184-8588, Japan
[b] Materials and Chemical Engineering, Group, School of Engineering, University of Greenwich, Medway, ME4 4TB, United Kingdom

ARTICLE INFO

Article history:
Received 29 October 2020
Received in revised form 1 December 2020
Accepted 8 December 2020
Available online xxxx

Keywords:
Calcium carbonate
Tensile strength
Thermal expansion
Nanoparticle
van der Waals force

ABSTRACT

Understanding the adhesiveness of fine particulate materials at high temperatures is important to achieving the stable, economical operation of various industrial systems. In the present research, two types of calcium carbonate ($CaCO_3$) particles having different mean particle sizes (often used as heat carriers in energy systems) were evaluated. The tensile strengths of beds of these materials were determined at various temperatures by tensile strength measurement tester. The adhesiveness was found to increase greatly at 500 °C even without chemical reactions or sintering, and X-ray diffraction analyses showed thermal expansion of the $CaCO_3$ crystals at 500 °C. Pure alumina (Al_2O_3) and silica (SiO_2) microparticles did not exhibit the same pronounced increases in tensile strength or crystal expansion at this same temperature. Because the surface distances between these primary particles were presumably small, it is proposed that van der Waals forces between the particles greatly increased at high temperatures. The addition of Al_2O_3 nanoparticles to the $CaCO_3$ decreased the tensile strengths of the powder beds both at ambient temperature and at 500 °C. The experimental data confirm that the surface distances between primary particles were increased upon incorporating the nanoparticles, such that the tensile strength decreased during heat treatment.

1. Introduction

Fine particulate materials are widely used in many industrial fields and the handling of these materials is a common source of various challenges. The adhesiveness of a powder, based on van der Waals forces or liquid bridges between particles, can significantly affect the ease of handling. Such effects are often enhanced at higher temperatures, which are frequently encountered during combustion, limestone calcination, chemical looping in post-combustion carbon dioxide (CO_2) capture processes, or fluidized reactors. The adhesiveness of a powder frequently increases in these cases, and can result in serious problems during the day-to-day operations of industrial facilities [1–6]. In particular, cohesive particles can deposit at various locations to form agglomerates, thus reducing heat recovery efficiency and blocking filters such that the flow of fluid streams is impeded [1,5]. Issues such as these related to the increased adhesiveness of powders are among the most serious long-term problems in energy plants, and tend to hinder the reliable and stable operation of such facilities. Since the mechanism responsible for increases in adhesiveness will vary with the physical properties of the particulate material (including chemical structure, particle diameter, and surface roughness) it is necessary to analyze the cause of adhesive forces that appear at various temperatures such that they can be controlled.

The tensile strength of a powder bed is a useful metric for evaluating the adhesive behavior of fine particulate materials. Several test procedures intended to determine the tensile strengths of powder beds have been developed over the last several decades, with tests typically performed at ambient temperature. However, the assessment of tensile strength at high temperatures remains a challenge [7–11]. In this regard, our group developed a split-type test device capable of measuring the tensile strength of a powder bed under high-temperature conditions [12]. In previous studies, this method was effectively used to analyze the adhesiveness of ash particles generated in combustion plants burning coal, biomass, and waste materials [13–16]. The adhesiveness of each of these ash powders, containing Si, Al, Na, K, and P compounds, was found to increase over the temperature range of 600–900 °C. This increased tensile strength was primarily attributed to liquid bridge forces resulting from the partial melting of eutectic phases on the

* Corresponding author.
E-mail address: kamiya@cc.tuat.ac.jp (H. Kamiya).

https://doi.org/10.1016/j.apt.2020.12.009

surfaces of the ash particles [15,17,18]. The porosity of the powder bed also had an important effect on tensile strength at high temperatures [14,16].

Rumpf's work provides a helpful approach to determining the tensile strength of ash powder beds at high temperatures [19]. On this basis, our group has attempted to regulate the adhesiveness and tensile strength of powders at high temperatures by adjusting porosity [14,16,18]. In previous studies, we were able to increase the porosity of powder beds by adding nanoparticle agents having a high degree of chemical stability at elevated temperatures to cohesive fine ash powders. This technique effectively suppressed adhesion at high temperatures and represents a new strategy for this purpose.

Calcium carbonate ($CaCO_3$) is widely used in many industries and recently has been effectively employed in sustainable chemical looping and CO_2 capture systems [20–25]. Usually in these systems, fuel gasification and CO_2 capture are performed in a gasifier furnace that is operated at either atmospheric pressure or pressurized condition and a temperature range of 600–700 °C. $CaCO_3$ is regenerated in a consequent regenerator furnace operated at 800–900 °C and atmospheric pressure conditions. However, pure $CaCO_3$ has been found to block pipes and beds in these systems at elevated temperatures. A liquid phase is not expected to be present during these processes, because the working temperatures are far below the melting point of the particles, and so the adhesiveness cannot be explained on the basis of liquid bridge forces. Evidently, the adhesiveness of $CaCO_3$ increases at the relative low temperatures in these systems via a unique mechanism. It is therefore important to characterize the fundamental adhesiveness of $CaCO_3$ particles. The resulting information regarding this pure material should also increase our fundamental understanding of the adhesiveness of more complex materials such as composites.

In the present work, the adhesiveness of pure cohesive $CaCO_3$ particles (several micrometers in diameter) was evaluated using a split-type tensile strength test device at temperatures ranging from ambient to 500 °C. The resulting data were compared with values for other pure materials such as silica and alumina. Based on further characterization, including X-ray diffraction (XRD) at high temperatures, a $CaCO_3$ adhesiveness mechanism is proposed and a method for controlling adhesiveness at high temperatures is detailed herein.

2. Material and methods

2.1. Materials

The commercially available $CaCO_3$ powders Eskal 300 and 500 (KSL Staubtechnik GmbH, Germany) were selected for this study because these materials provided suitable purity and particle size ranges. Details regarding these specimens are presented in Table 1, Fig. S1 and Fig. S2 in Supporting Information (SI). These materials had average particle sizes of 2.2 and 4.4 μm, respectively, and are referred to herein as $CaCO_3$–2 μm and $CaCO_3$–4 μm, respectively. Al_2O_3 microparticles (AA-3, Sumitomo Chemical Co., Ltd., average particle size = 3.0 μm) and SiO_2 microparticles (FB6S, Denka Co., Ltd., average particle size = 5.7 μm) were also evaluated for comparison purposes, and detailed information regarding these samples is included in Table 1, Fig. S1 and Fig. S2. In some trials, Al_2O_3 nanoparticles (AEROXIDE Alu 130, Nippon Aerosil) were used as an additive to adjust adhesiveness. Details of these nanoparticles are included in Table S1 as well as Figs. S3 – S6. These Al_2O_3 nanoparticles were added to the $CaCO_3$ at 3 wt% by simple mixing under air.

2.2. Measurement of the tensile strengths of the powder beds

The tensile strengths of $CaCO_3$, Al_2O_3, and SiO_2 powder beds were assessed using a split-type test device under air at temperatures ranging from ambient to 500 °C. Details of the test apparatus and test conditions are provided in Fig. S7 and Table S2. Each powder bed was prepared by packing a 6–10 g sample (the volume of powder bed was 8–10 cm^3) into a cylindrical cell (diameter 50 mm × height 10 mm) followed by uniaxial pressing at 2.1 kPa for 10 min. The cell containing the powder bed was subsequently heated to a target temperature ranging from 25 to 500 °C at a heating rate of 20 °C/min and held at that temperature for 30 min before measurement of the tensile strength. After determining the tensile strength, the volume of the bed was determined to allow the packing density and porosity to be calculated.

2.3. Characterization

The particle size distribution of the samples was measured by a laser particle size analyzer (Horiba, LA-950ND) in a dry system. The thermal properties of the samples were determined by thermogravimetry–differential thermal analysis (TG–DTA, Rigaku, Thermo plus EVO TG8120) and thermomechanical analysis (TMA, Rigaku, TMA8310) under air at a heating rate of 10 °C/min. The crystalline structures of the samples were analyzed by XRD (Rigaku, RINT 2100 VPC/N) at a target temperature ranging from 25 to 500 °C under air. In these trials, each sample was placed on a platinum plate and heated to the target temperature at 20 °C/min, after which the specimen was held at that temperature for 10 min before acquiring data. XRD analysis were carried out with scan speed of 5°/min at a measurement interval of 0.05°. A Cu Kα X-ray source was used with X-ray tube voltage and current of 40 kV and 30 mA, respectively.

2.4. Theoretical analysis

Thermodynamic calculations were carried out using the FactSage 7.3 software package and the FTOxid and FactPS databases.

Table 1
Physical properties of the materials used in this research.

Sample	Particle size/μm	Particle density/kg m^{-3}	Packing density at room temperature/kg m^{-3}[c]	Powder bed porosity at room temperature[c]
Eskal 300 ($CaCO_3$–2 μm)	2.2[a]	2853	719	0.748
Eskal 500 ($CaCO_3$–4 μm)	4.4[a]	2868	860	0.700
SiO_2 microparticles	3.0[b]	3975	1455	0.634
Al_2O_3 Microparticles	5.7[b]	2368	794	0.659

[a] Determined using a RODOS instrument (Sympatec GmbH).
[b] Determined by field emission scanning electron microscopy image analysis.
[c] A 6–10 g sample was packed into a cylindrical cell (50 mm) and consolidated by uniaxial pressing (2.1 kPa) for 10 min at room temperature.

3. Results and discussion

The tensile strengths of the $CaCO_3$, Al_2O_3, and SiO_2 beds were measured at various temperatures, with the results presented in Fig. 1. At ambient temperature, the tensile strengths were relatively low (0.20 and 0.16 kPa for the $CaCO_3$–2 μm and $CaCO_3$–4 μm, respectively) but increased beginning at 200 and 300 °C, respectively. Gradual strength increases were observed with further temperature increases. Moreover, the tensile strengths of the $CaCO_3$–2 μm and $CaCO_3$–4 μm beds exhibited an increase at 500 °C (to 2.8 and 2.7 kPa for the $CaCO_3$–2 μm and $CaCO_3$–4 μm, respectively). The tensile strengths of the Al_2O_3 and SiO_2 increased with a rise beginning at 400 °C, but the run ratios were smaller than for $CaCO_3$. Fig. 2 depicts the comparison of tensile strengths values obtained for $CaCO_3$, Al_2O_3, and SiO_2 beds between ambient temperature and 500 °C. The tensile strength values of these materials represent increasing factors of 13 and 16, respectively. In contrast, the Al_2O_3 and SiO_2 microparticles (Fig. 2) showed only approximately threefold increases in tensile strength on going from ambient temperature to 500 °C.

Thermal analysis of the $CaCO_3$ materials (Fig. 3) indicated decomposition over the range of 600–800 °C, in agreement with reported behavior for this compound. A careful analysis of the data also suggests shrinkage, beginning at 800 °C, but no changes in mass or volume up to 500 °C. Up to this temperature, Al_2O_3 and SiO_2 did not show changes in mass or volume. Neither sintering nor chemical reactions appear to have occurred below 500 °C. Considering both the tensile strength and thermal analysis data, phenomena other than sintering and chemical reactions might be responsible for the increased tensile strength of the powder beds at 500 °C, which could explain the different behavior of the $CaCO_3$ samples compared with the Al_2O_3 and SiO_2.

Liquid phase formation and diffusion did not take place in the $CaCO_3$ specimens up to 500 °C, and therefore the primary mechanism responsible for adhesion between particles might be van der Waals forces, F_v. When only van der Waals forces act between particles, the tensile strength of the powder bed, σ, can be explained by following equation according to Rumpf's work [19]:

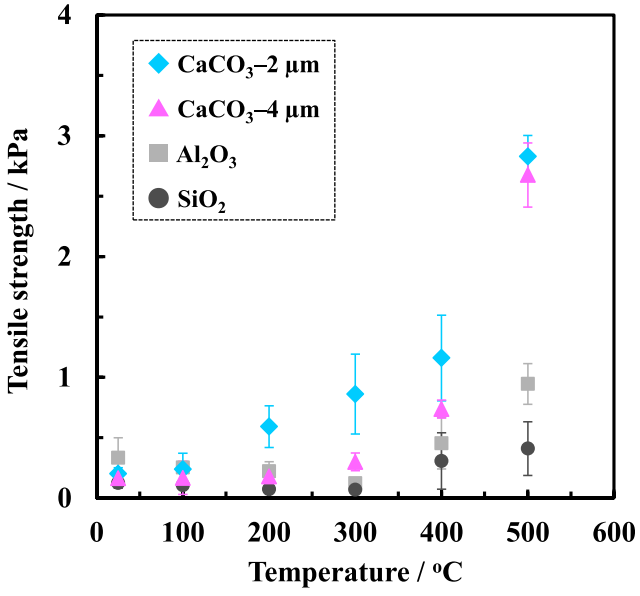

Fig. 1. Tensile strengths of the $CaCO_3$–2 μm (◆), $CaCO_3$–4 μm (▲), Al_2O_3 (■) and SiO_2 (●) powder beds as functions of temperature. Error bars correspond to standard variation.

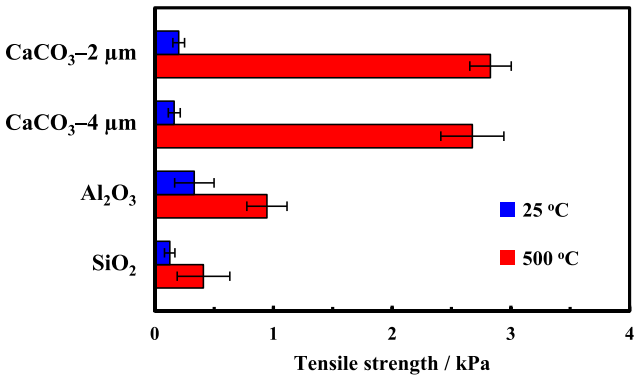

Fig. 2. Comparison of the tensile strengths of different powder beds at 25 °C (blue) and 500 °C (red). (For interpretation of the references to colour in this figure legend, the reader is referred to the web version of this article.)

$$\sigma = \frac{1-\varepsilon}{\varepsilon}\frac{F_v}{x^2} \tag{1}$$

where ε is the porosity of the powder bed. And the distance between particle surfaces, H, can be estimated based on the following equation:

$$\sigma = \frac{1}{24}\frac{1-\varepsilon}{\varepsilon}\frac{A}{H^2 x} \tag{2}$$

where A is the Hamaker constant, and x is the average particle size. The Hamaker constant can be obtained using the method reported by Bergström [26] and the values obtained in the present study were 9.43×10^{-20} and 9.73×10^{-20} J at 25 and 500 °C, respectively (see SI for details of the calculations). Since the thermal analysis did not reveal any variations in the mass or height of the powder beds below 500 °C, the porosity evidently remained constant despite the rise in temperature. Therefore, we assumed that only the distances between particle surfaces varied with temperature, and these distances were calculated. At ambient temperature, these intervals were estimated to be 1.7 and 1.5 nm for the $CaCO_3$–2 μm and $CaCO_3$–4 μm, respectively. Also assuming that the tensile strength was inversely proportional to the distance, increasing the temperature from ambient to 500 °C would be expected to decrease these values by 70% and 75% for the $CaCO_3$–2 μm and $CaCO_3$–4 μm, respectively.

Thermal expansion typically occurs in materials at high temperatures and is frequently unrelated to chemical reactions. The crystalline thermal expansions of the specimens in this work were examined by acquiring XRD patterns during heat treatment (Fig. 4). Note that, because the SiO_2 microparticles used in this research had an amorphous structure, they were not assessed. The patterns obtained from the $CaCO_3$ were assigned to a calcite crystal structure and this structure did not change heating up to 500 °C, although the diffraction peaks were slightly shifted in the negative direction. As an example, the peak at approximately 29.4° assigned to the [104] lattice plane in $CaCO_3$ was shifted –0.17° and –0.16° for the $CaCO_3$–2 μm and $CaCO_3$–4 μm, respectively. This result indicates increases in the lattice plane distances. The [104] plane distances (d_{104}) were also calculated. At 25 °C, the distances ($d_{104,\ 25}$) were estimated to be 3.035 and 3.023 Å for the $CaCO_3$–2 μm and $CaCO_3$–4 μm, respectively, while at 500 °C the distances ($d_{104,\ 500}$) increased to 3.052 and 3.039 Å, respectively. The same analysis was carried out for the Al_2O_3 microparticles and no changes in crystal structure were observed upon heat treatment, although there was a slight negative shift of the peaks at 500 °C. The extent of this shift was significantly smaller than that in the $CaCO_3$ patterns (with a shift of the peak at approximately 35.2°, assigned to the [104] lattice plane, of –0.12°). As a result,

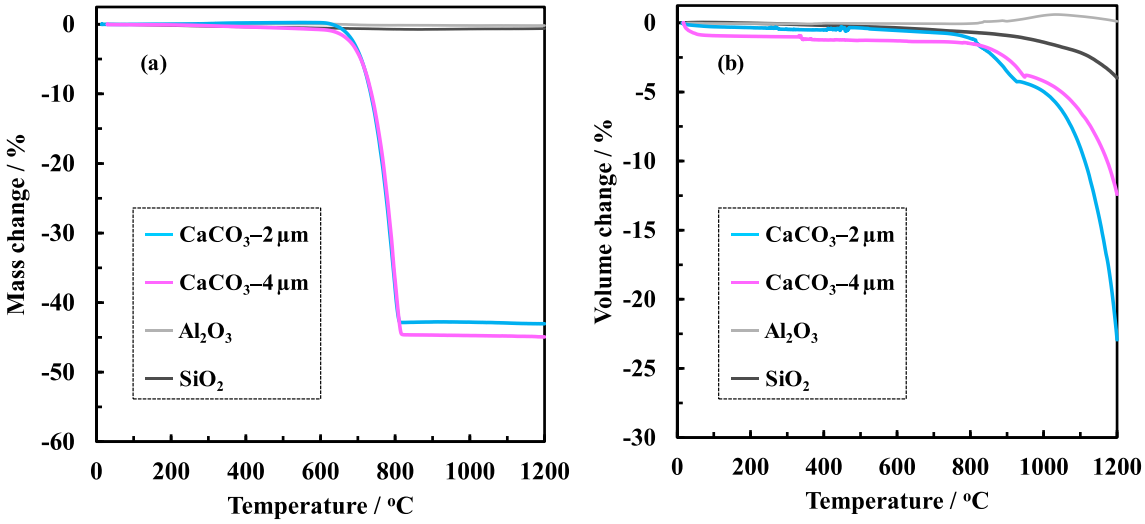

Fig. 3. Thermal analysis data for the $CaCO_3$, Al_2O_3 and SiO_2 samples. (a) TG and (b) TMA plots acquired at a heating rate of 10 °C/min under air.

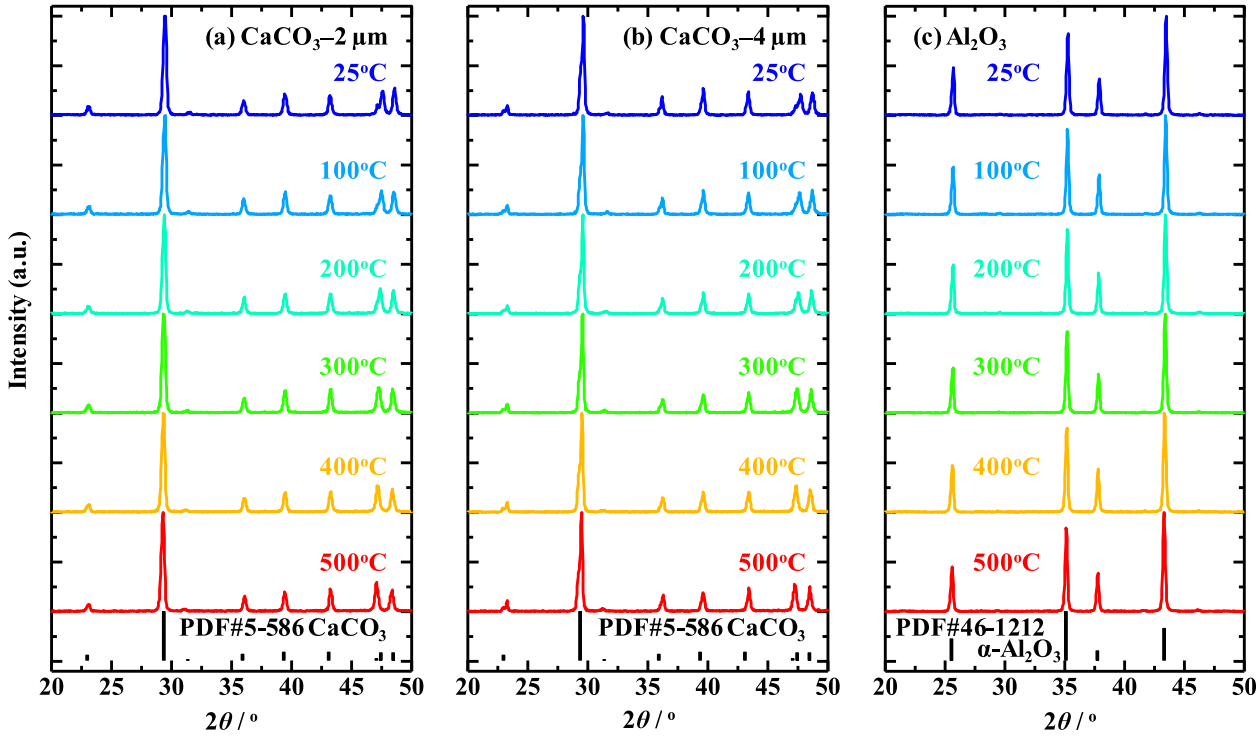

Fig. 4. XRD patterns obtained from the (a) $CaCO_3$–2 μm, (b) $CaCO_3$–4 μm, and (c) Al_2O_3 at temperatures ranging from 25 to 500 °C together with patterns based on ICDD cards.

the change in d_{104} was also smaller than those for the $CaCO_3$, with $d_{104,\ 25}$ and $d_{104,\ 500}$ of 2.546 and 2.555 Å, respectively. The lattice plane distances were estimated at each temperature and the linear increase of the distances with temperature were observed (Fig. 5). The slopes for these increases for $CaCO_3$ were larger than that for Al_2O_3. It was observed that surface distances calculated from tensile strengths decreased with respect to the temperature increase (Fig. S8) We postulate that these reductions were induced by the proportional increase of lattice plane distances. Furthermore, since the distances at ambient temperature after heat treatment were same as before heating (Fig. S9), these increases were able to be observed under high temperature conditions. There have been several reports to date that the thermal expansion coefficient of $CaCO_3$ is 25×10^{-6} K^{-1}, which is significantly higher than the values for Al_2O_3 (5×10^{-6} K^{-1}) and SiO_2 (0.55×10^{-6} K^{-1}) [27–29]. Thus, $CaCO_3$ will tend to expand to a greater extent compared with Al_2O_3 and SiO_2 at high temperatures, in agreement with our XRD results. Based on this comparison of $CaCO_3$ with Al_2O_3, we suggest that materials showing greater adhesiveness at high temperatures may also expand more readily.

The volume expansion of the powder beds could have been induced by microscopic crystalline expansions, but the TMA data in Fig. 3 do not show thermal expansion of the $CaCO_3$ powder beds. Therefore, it is possible that the $CaCO_3$ particles approached one another due to the thermal expansion of the crystals. Decreases in the distances between particle surfaces would be expected to increase the van der Waals forces, which would also increase the tensile strengths of the powder beds. We therefore concluded that

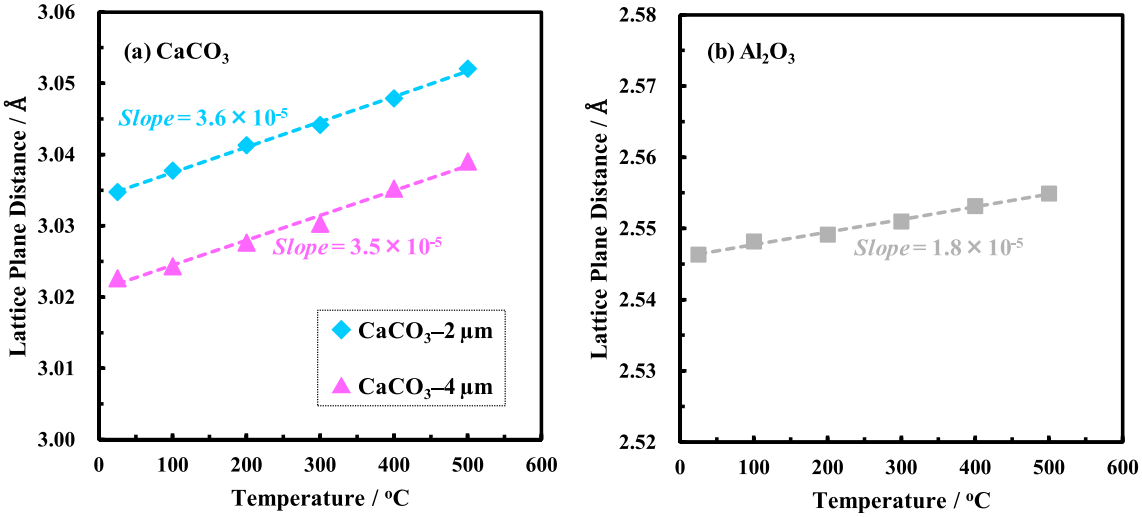

Fig. 5. [104] lattice plane distances for $CaCO_3$–2 μm (◆), $CaCO_3$–4 μm (▲) and Al_2O_3 (■) as functions of temperature.

the thermal expansion of the $CaCO_3$ crystals at high temperatures produced the observed increases in tensile strength.

In another series of tests, we attempted to adjust the tensile strengths of the $CaCO_3$ powder beds at high temperatures via the addition of Al_2O_3 nanoparticles (Al_2O_3–NPs). In a previous study, the addition of Al_2O_3–NPs to coal particles and sewage sludge ashes increased the porosities of the powder beds while decreasing the tensile strengths at high temperatures.[14,16] To confirm a similar effect, Al_2O_3–NPs were added to the $CaCO_3$ particles at 3 wt% and the tensile strengths of the powder beds were determined at ambient temperature and 500 °C, with the results provided in Fig. 6. At ambient temperature, the Al_2O_3–NPs decreased the tensile strengths of the $CaCO_3$–2 μm and $CaCO_3$–4 μm by 40% and 26%, respectively. The effect of the Al_2O_3–NPs was even more remarkable at 500 °C, with tensile strength decreases of 64% and 74%, respectively. Fig. 7 plots the porosity values of the $CaCO_3$ powder beds with and without the Al_2O_3–NPs. As expected, incorporating the Al_2O_3–NPs increased the porosities of the beds, suggesting that poor packing was induced.

According to these observations and considering the Rumpf model, tensile strength decreases of 35% and 34% would be expected for the $CaCO_3$–2 μm and $CaCO_3$–4 μm, respectively, which are relatively close to the actual decreases at ambient temperature. Thus, there was reasonable agreement between the porosity and tensile strengths obtained experimentally and the values estimated theoretically (Fig. 8 (a)). Therefore, we concluded that the decreased tensile strengths at ambient temperatures resulted from decreases in the porosity of each powder bed. In contrast, the proportionate decreases in the tensile strengths following the addition of Al_2O_3–NPs at 500 °C were higher than the estimated values based on the porosity increases (Fig. 8 (b)). The XRD data demonstrated that neither the incorporation of Al_2O_3–NPs nor the heat treatment changed the crystal structures (see Fig. S10). Thermodynamic calculations for the binary $CaCO_3$-Al_2O_3 systems also showed that these compounds would not be expected to react below 500 °C (see SI for details and results regarding these calculations). These findings demonstrate an effect other than a chemical reaction, likely related to the increased porosity that appears to have decreased the tensile strengths of the $CaCO_3$ powder beds at 500 °C following the addition of the Al_2O_3–NPs. As noted, the increased tensile strengths of the beds at high temperatures were attributed to decreases in the inter-particle distances. We propose that the addition of Al_2O_3–NPs to the $CaCO_3$ powder beds increased

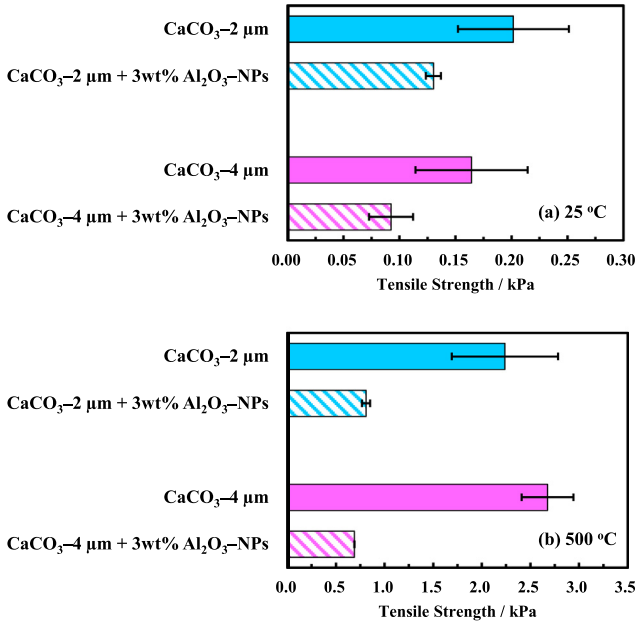

Fig. 6. Tensile strengths of powder beds of $CaCO_3$ with Al_2O_3 nanoparticles (Al_2O_3–NPs) at (a) 25 and (b) 500 °C.

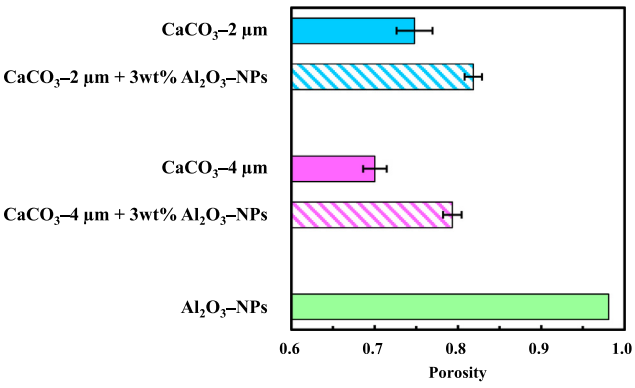

Fig. 7. Porosities of powder beds of $CaCO_3$ with and without Al_2O_3 nanoparticles (Al_2O_3–NPs) and of the original Al_2O_3–NPs.

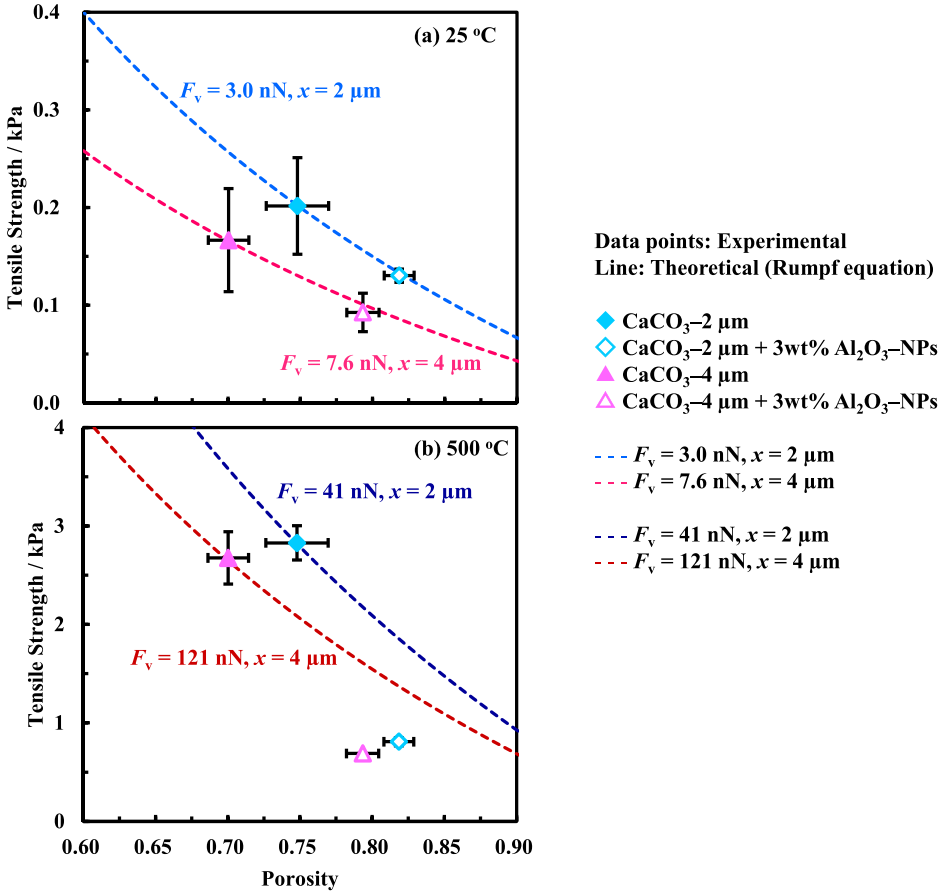

Fig. 8. Tensile strengths of powder beds as functions of porosity, based on experimental data (plotted points) and the Rumpf equation (dashed lines) at (a) 25 and (b) 500 °C. F_v accounts for the van der Waals force which was re-calculated backwards from the tensile strength using the Rumpf model (equation (1)).

the distances between $CaCO_3$ particles by a lubricant effect attributed to filling of the interstitial voids between particles and/or a rolling effect during packing of particles at ambient temperature. Elemental mapping by energy-dispersive X-ray spectroscopy (Fig. S11) indicated that the Al_2O_3–NPs were located on the surfaces of the original $CaCO_3$ microparticles. Therefore, when the beds containing Al_2O_3–NPs and $CaCO_3$ particles were packed, the Al_2O_3–NPs filled the spaces between the $CaCO_3$ microparticles and separated the particles.

4. Conclusions

The adhesiveness of cohesive $CaCO_3$ microparticles was ascertained at high temperatures using a tensile strength tester. The tensile strengths of these materials clearly increased at higher temperatures, but this effect was not attributed to chemical reactions or sintering. XRD analyses at high temperatures indicated thermal expansion of the $CaCO_3$ crystals. These results suggested that the distances between particle surfaces were reduced such that van der Waals forces were increased. In contrast, the degrees of thermal expansion and the increases in tensile strength at high temperatures of Al_2O_3 and SiO_2 microparticles were very moderate. The high tensile strengths of the $CaCO_3$ powder beds were therefore ascribed to the high thermal expansion coefficient of this material. The addition of Al_2O_3 nanoparticles to the $CaCO_3$ lowered the tensile strengths both at ambient and high temperatures while increasing the porosities of the powder beds. This occurred due to the poor packing induced by the nanoparticles and increased the inter-particle distances at high temperatures.

Declaration of Competing Interest

The authors declare that they have no known competing financial interests or personal relationships that could have appeared to influence the work reported in this paper.

Acknowledgements

The authors are grateful to Professor Emeritus Masayuki Horio for helpful technical advice during the preparation of this manuscript. This work was supported by JSPS KAKENHI grant number 18H05342.

Appendix A. Supplementary material

Supplementary data to this article can be found online at https://doi.org/10.1016/j.apt.2020.12.009.

References

[1] M.A. Souto, J.C. Rodriguez, R. Conde-Pumpido, F. Guitián, J.F. Gonzalez, J. Perez, Formation of solid deposits in the gas circuit of a pressurized fluidized bed combustion plant, Fuel 75 (1996) 675–680.
[2] M. Tsukada, K. Kawashima, H. Yamada, Y. Yao, H. Kamiya, Analysis of adhesion behavior of waste combustion ash at high temperatures and its control by the addition of coarse particles, Powder Technol. 180 (2008) 259–264.
[3] X. Wang, Y. Liu, H. Tan, L. Ma, T. Xu, Mechanism research on the development of ash deposits on the heating surface of biomass furnaces, Ind. Eng. Chem. Res. 51 (2012) 12984–12992.
[4] Q. Zhang, H. Liu, Y. Qian, M. Xu, W. Li, J. Xu, The influence of phosphorus on ash fusion temperature of sludge and coal, Fuel Process. Technol. 110 (2013) 218–226.

[5] X. Wu, X. Zhang, K. Yan, N. Chen, J. Zhang, X. Xu, B. Dai, J. Zhang, L. Zhang, Ash deposition and slagging behavior of Chinese Xinjiang high-alkali coal in 3 MW_{th} pilot-scale combustion test, Fuel 181 (2016) 1191–1202.
[6] Y.J. Lee, J.W. Choi, J.H. Park, H. Namkung, G.S. Song, S.J. Park, D.W. Lee, J.G. Kim, C.H. Jeon, Y.C. Choi, Techno-economical method for the removal of alkali metals from agricultural residue and herbaceous biomass and its effect on slagging and fouling behavior, ACS Sustainable Chem. Eng. 6 (2018) 13056–13065.
[7] R. Farley, F.H.H. Valentin, Problems associated with storage hoppers, Trans. Inst. Chem. Eng. 43a (1965) 193–198.
[8] J. Tsubaki, G. Jimbo, Theoretical analysis of the tensile strength of a powder bed, Powder Technol. 37 (1984) 219–227.
[9] J.P. Hurley, B.A. Dockter, Factors affecting the tensile strength of hot-gas filter dust cakes, Adv. Powder Technol. 14 (2003) 695–705.
[10] Y. Lexminarayan, A.B. Nair, P.A. Jensen, H. Wu, F.J. Frandsen, B. Sander, P. Glarborg, Tensile adhesion strength of biomass ash deposits: effect of the temperature gradient and ash chemistry, Energy Fuels 32 (2018) 4432–4441.
[11] P. García-Triñanes, S. Luding, H. Shi, Tensile strength of cohesive powders, Adv. Powder Technol. 30 (2019) 2868–2880.
[12] H. Kamiya, A. Kimura, T. Yokoyama, M. Naito, G. Jimbo, Development of a split-type tensile-strength tester and analysis of mechanism of increase of adhesion behavior of inorganic fine powder bed at high-temperature conditions, Powder Technol. 127 (2002) 239–245.
[13] M. Tsukada, H. Yamada, H. Kamiya, Analysis of biomass combustion ash behavior at elevated temperatures, Adv. Powder Technol. 14 (2003) 707–717.
[14] G. Horiguchi, R. Fujii, Y. Yamauchi, H. Okabe, M. Tsukada, Y. Okada, H. Kamiya, Toward stable operation of coal combustion plants: the use of alumina nanoparticles to prevent adhesion of fly ash, Energy Fuels 32 (2018) 13015–13020.
[15] J. Gao, M. Matsushita, G. Horiguchi, R. Fujii, M. Tsukada, Y. Okada, H. Kamiya, Toward stable operation of sewage sludge incineration plants: the use of alumina nanoparticles to suppress adhesion of fly ash, Energy Fuels 33 (2019) 9363–9366.
[16] M. Ito, G. Horiguchi, T. Hariu, A. Ito, H. Kamiya, Y. Okada, Controlling fly ash adhesion at high temperatures via porosity effect, Powder Technol. 374 (2020) 492–495.
[17] H. Kamiya, A. Kimura, M. Tsukada, A. Naito, Analysis of the high-temperature cohesion behavior of ash particles using pure silica powders coated with alkali metals, Energy Fuels 16 (2002) 457–461.
[18] G. Horiguchi, R. Fujii, Y. Beppu, H. Kamiya, Y. Okada, Understanding the mechanism of particle adhesion in high temperature combustion induced by sodium and potassium: use of a synthetic ash strategy, Ind. Eng. Chem. Res. 59 (2020) 16185–16190.
[19] H. Rumpf, On the theory of tensile strength of agglomerates during force transmission at contact points, Chem. Ing. Tech. 42 (1970) 538–540.
[20] X. Zhao, H. Zhou, V.S. Sikarwar, M. Zhao, A.A. Park, P.S. Fennell, L. Shen, L.S. Fan, Biomass-based chemical looping technologies: the good, the bad and the future, Energy Environ. Sci. 10 (2017) 1885–1910.
[21] D. Choi, J. Shin, Y. Park, Effects of CaCl2 on cyclic carbonation-calcination kinetics of CaO-based composite for potential application to solar thermochemical energy storage, Chem. Eng. J. 130 (2021) 116207.
[22] J.D. Durán-Martín, P.E. Sánchez Jimenez, J.M. Valverde, A. Perejón, J. Arcenegui-Troya, P. García Triñanes, L.A. Pérez Maqueda, J. Adv. Res. 22 (2020) 67–76.
[23] S. Lin, M. Harada, Y. Suzuki, H. Hatano, Process analysis for hydrogen production by reaction integrated novel gasification (HyPr-RING), Energy Convers. Manag. 46 (2005) 869–880.
[24] G. Soukup, C. Pfeifer, A. Kreuzeder, H. Hofbauer, In situ CO_2 capture in a dual fluidized bed biomass steam gasifier – bed material and fuel variation, Chem. Eng. Technol. 32 (2009) 348–354.
[25] J. Udomsirichakorn, P. Basu, P.A. Salama, B. Acharya, CaO-based chemical looping gasification of biomass for hydrogen-enriched gas production with in situ CO_2 capture and tar reduction, Fuel Process. Technol. 127 (2014) 7–12.
[26] L. Bergström, Hamaker constants of inorganic materials, Adv. Colloid Interface Sci. 70 (1997) 125–169.
[27] K.V.K. Rao, S.V.N. Naidu, K.S. Murthy, Precision lattice parameters and thermal expansion of calcite, J. Phys. Chem. Solids 29 (1968) 245–248.
[28] M. Cavillon, P.D. Dragic, J. Ballato, Additivity of the coefficient of thermal expansion in silicate optical fibers, Opt. Lett. 42 (2017) 3650–3653.
[29] S. Chatterjee, B.N. Chowdhury, A. Das, S. Chattopadhyay, Estimation of step-by-step induced stress in a sequential process integration of nano-scale SOS MOSFETs with high-k gate dielectrics, Semicond. Sci. Technol. 28 (2013) 125011–125017.